INGRID: Intelligent Generative Robotic Design Using Large Language Models

Guanglu Jia[a,†], Ceng Zhang[a,†], Gregory S. Chirikjian[b,*]

[a] Department of Mechanical Engineering, College of Design and Engineering, National University of Singapore, Singapore, 117575, Singapore
[b] Department of Mechanical Engineering, University of Delaware, Newark, DE 19716, United States

Abstract

The integration of large language models (LLMs) into robotic systems has accelerated progress in embodied artificial intelligence, yet current approaches remain constrained by existing robotic architectures, particularly serial mechanisms. This hardware dependency fundamentally limits the scope of robotic intelligence. Here, we present INGRID (Intelligent Generative Robotic Design), a framework that enables the automated design of parallel robotic mechanisms through deep integration with reciprocal screw theory and kinematic synthesis methods. We decompose the design challenge into four progressive tasks: constraint analysis, kinematic joint generation, chain construction, and complete mechanism design. INGRID demonstrates the ability to generate novel parallel mechanisms with both fixed and variable mobility, discovering kinematic configurations not previously documented in the literature. We validate our approach through three case studies demonstrating how INGRID assists users in designing task-specific parallel robots based on desired mobility requirements. By bridging the gap between mechanism theory and machine learning, INGRID enables researchers without specialized robotics training to create custom parallel mechanisms, thereby decoupling advances in robotic intelligence from hardware constraints. This work establishes a foundation for mechanism intelligence, where AI systems actively design robotic hardware, potentially transforming the development of embodied AI systems.

Introduction

The integration of artificial intelligence (AI) into robotics has fundamentally transformed control strategies for autonomous systems, enabling unprecedented capabilities in uncertain environments [1]. Recent advances in embodied AI have demonstrated its effectiveness across a wide range of robotic applications. In locomotion control, Nygaard et al. enabled quadrupedal robots to adapt to unstructured environments [2], while Jin et al. introduced imitation-relaxation reinforcement learning to optimize high-speed quadrupedal robot objectives [3]. Thor and Manoonpong proposed modular neural control structures with fast learning for legged robots [4], and Yu et al. presented a systematic saliency analysis for motor skills learned through deep reinforcement learning [5]. Han et al. developed a hierarchical framework for constructing reusable knowledge at primitive, environmental, and strategic levels [6], while Stella et al. introduced passive automata with synergies for more efficient robotic locomotion [7].

Beyond locomotion, AI has revolutionized tactile robot skills [8], robot collaboration tasks [9], and human-robot interaction [10, 11]. Li et al. proposed interactive robot controllers that induce human-robot interaction strategies [12], and Mintchev et al. designed force feedback systems for human-robot interactions [13]. Massari et al. developed convolutional neural network approaches for safe human-robot cooperation through machine intelligence [14], while Hu et al. introduced self-supervised learning frameworks enabling robots to model their morphology, kinematics, and motor control [15].

The application of AI extends to complex control problems across robotic domains. Ju et al. applied sim-to-real transfer reinforcement learning methods to solve real-world robot control challenges [16]. Luo et al. described closed user-in-the-loop control frameworks for construction assembly robots based on large language model (LLM) techniques [17]. Schmidgall et al. outlined pathways for building general-purpose machine learning models for robot-assisted surgery [18]. Mon-Williams et al. proposed an embodied large-language-model-enabled robot (ELLMER) framework for completing complex tasks in uncertain environments [19], and Wu et al. developed trustworthy AI frameworks integrated with LLMs for natural language robot control [20].

---

† These authors contributed equally to this work.
* Corresponding author.
E-mail address: gchirik@udel.edu (G.S. Chirikjian).

Despite the rapid development of LLMs in robotics, their application to robotic mechanism design remains limited. This gap between LLMs and mechanism design represents a critical challenge that needs to be addressed to fully realize the potential of AI in robotics.

Human researchers have developed multiple systematic approaches for synthesizing robotic mechanisms. The screw-based method employs reciprocal screw theory to construct parallel mechanism families by combining motion-screws derived from constraint conditions. Huang and Li pioneered the synthesis of lower-mobility parallel robots using the general Grübler-Kutzbach criterion [21, 22]. This foundation enabled the synthesis of diverse parallel robots: spatial parallel manipulators [23], decoupled rotational parallel mechanisms [24], single degree-of-freedom (DOF) multi-mode parallel mechanisms [25], 2T1H parallel mechanisms without helical joints [26], 3-RSR equivalent 2R1T parallel mechanisms [27]. metamorphic parallel robots [28], mobile parallel mechanisms [29], and 2R2T hybrid mechanisms [30].

Group-based methods offer an alternative approach. Li et al. designed parallel mechanisms with bifurcation of Schoenflies motion [31, 32] and 3-DOF RPR equivalent parallel mechanisms [33]. Xing et al. utilized Lie group theory for reconfigurable generalized parallel manipulators [34], while Wei and Dai designed configurable parallel mechanisms capable of switching between spherical and planar motion [35].

Topology-based methods analyze mechanisms through structural principles. Yazici et al. proposed synthesis methodologies for platform-type manipulators based on topology representation [36]. Xia et al. synthesized continuous origami mechanisms using topological graph theory [37, 38], Lin et al. designed hybrid remote center motion mechanisms through topological arrangement [39], and Archer and Hopkins introduced visualization-based methods for constructing interconnected hybrid mechanisms [40].

Kinematics-based methods leverage kinematic analysis for mechanism design. Zhao et al. developed type synthesis methods based on the Jacobian matrix [41]. Xia et al. designed decoupled generalized parallel mechanisms through motion transmission [42], and Tian et al. created reconfigurable parallel mechanisms by introducing kinematic redundancy [43]. Liu et al. synthesized self-alignment parallel ankle rehabilitation robots based on ankle joint kinematic characteristics [44], and Liu et al. developed design methods for 3-DOF cable-driven parallel robots through workspace analysis [45].

However, these established methods present significant barriers to non-specialists. The mathematical complexity and domain expertise required for mechanism synthesis limit innovation to a small community of specialists. Moreover, most existing synthesis methods address either fixed-mobility or variable-mobility mechanisms in isolation, lacking a unified framework that can seamlessly transition between these categories based on design requirements.

We present INGRID (Intelligent Generative Robotic Design), a system that combines LLMs with screw theory to enable automated synthesis of parallel robotic mechanisms. We selected screw theory as our foundation because screws effectively describe kinematic joints and facilitate combination and derivation operations suitable for LLM processing. Like words constructing phrases and sentences in language models, or DNA sequences forming proteins in biological systems, kinematic joints construct chains that form robotic mechanisms—with INGRID encoding the rules for this construction process. Our approach addresses three critical challenges in current robotic design:

First, INGRID bridges the gap between natural language and robotic mechanism design. Recognizing that most computer science researchers lack expertise in mechanism design, we developed a method that enables LLMs to assist users in designing desired robotic mechanisms without specialized knowledge, significantly lowering the design threshold.

Second, our system specifically targets parallel mechanisms, an underexplored domain in AI-driven robotics despite their advantages for high-precision tasks, heavy payload manipulation, and applications requiring high stiffness-to-weight ratios. This focus complements the predominant emphasis on serial robots in current embodied AI research, expanding the scope of AI-driven robotics.

Third, INGRID provides a unified framework for designing both fixed-mobility and variable-mobility parallel mechanisms through a consistent methodology. By establishing connections between motion screws and kinematic joints within a generative model, our system can synthesize mechanisms ranging from conventional parallel robots (fixed mobility) to reconfigurable systems (variable mobility) that adapt their mobility based on requirements.

In summary, we establish a generative model for designing parallel robotic mechanisms through a language-based interface, addressing LLM shortcomings in mechanism design. This work realizes mechanism intelligence and paves the way for advancing robotic AI by enabling automated design of the physical structure.

Results

The INGRID workflow for parallel robotic mechanism design

We present INGRID, an intelligent design system that systematically addresses the synthesis of parallel robotic mechanisms through four integrated computational tasks (Fig. 1): (Task A) Analysis of Constraint Conditions, (Task B) Linear Combination of Screws, (Task C) Construction of Kinematic Chains, and (Task D) Design of Robotic Mechanisms.

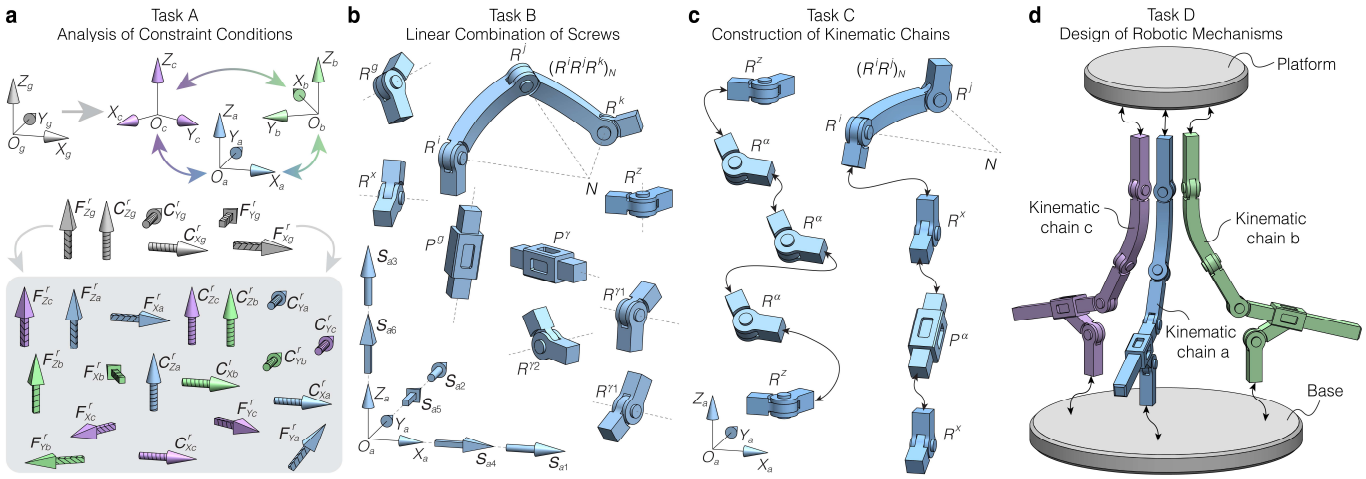

Fig. 1. The workflow of INGRID. **(a)** Task A: INGRID provides constraint conditions based on the global coordinate frame (grey) and local coordinate frames (blue, green, and purple). Subsequently, INGRID determines the desired constraint conditions for each local coordinate frame. **(b)** Task B: INGRID generates new kinematic joints based on the local coordinate frame. **(c)** Task C: INGRID constructs new kinematic chains using the candidate kinematic joints from Task B. **(d)** Task D: INGRID completes the design of parallel robotic mechanisms using the potential kinematic chains.

In Task A, the system initiates an interactive design process through the following sequential steps:

Step A1: Selection of the desired robotic mechanism type.
Step A2: Specification of mobility requirements.
Step A3: Definition of degrees of freedom (DOFs) for the kinematic chain.
Step A4: Derivation of constraint conditions based on user specifications.

In this task, INGRID establishes the relationship between the global coordinate frame $\{O_g\text{-}X_gY_gZ_g\}$ and three local coordinate frames $\{O_a\text{-}X_aY_aZ_a\}$, $\{O_b\text{-}X_bY_bZ_b\}$, and $\{O_c\text{-}X_cY_cZ_c\}$. The system analyzes constraint conditions by transforming them into constraint forces and couples (Fig. 1a), enabling systematic identification of constraints within each local coordinate frame.

Building upon the constraint analysis, Task B employs screw theory to generate new kinematic joints through the following procedure:

Step B1: Derivation of the standard base for the motion-screw system.
Step B2: Linear combinations utilizing revolute-joint-screws.
Step B3: Linear combinations employing prismatic-joint-screws.
Step B4: Hybrid combinations integrating single revolute-joint-screws with prismatic-joint-screws.
Step B5: Complex combinations involving multiple revolute-joint-screws with prismatic-joint-screws.
Step B6: Synthesis and categorization of combination results.

This systematic approach generates a comprehensive set of potential kinematic joints (Fig. 1b) within the local coordinate framework, providing the foundation for subsequent kinematic chain construction. Then, Task C synthesizes kinematic chains through exhaustive permutation analysis:

Step C1: Identification of available kinematic joints and sub-chains.
Steps C2-C5: Systematic analysis based on prismatic joint count (from three to zero).
Step C6: Compilation of new kinematic chain configurations.

The system constructs kinematic chains by strategically connecting the generated kinematic joints (Fig. 1c), ensuring kinematic compatibility and satisfying the required constraints. Task D represents the final stage, in which INGRID transforms kinematic chains into complete parallel robotic mechanisms:

Step D1: Generation of all feasible permutations based on user selections.
Step D2: Physical interpretation of each valid configuration.
Step D3: Guidance on locating the URDF file for simulation and implementation.

Users select configurations based on prismatic joint requirements, enabling INGRID to construct the complete parallel mechanism by connecting kinematic chains through appropriate platforms and bases. The system provides the configuration of the new kinematic chain, guides us in constructing the mechanism structure, and generates the URDF files for direct integration into robotic simulation environments.

Constraint analysis framework (Task A)

Geometric configuration of coordinate frames. We consider parallel mechanisms comprising three kinematic chains positioned at local coordinate frames $\{O_i\text{-}X_iY_iZ_i\}$ where $i \in \{a, b, c\}$. The Z_i-axes are constrained parallel to the Z_g-axis (perpendicular to the base), defining auxiliary planes a, b, and c. Four fundamental geometric configurations emerge: (1) **non-collinear intersection**: Auxiliary planes intersect without sharing a common line (Fig. 2a). (2) **Collinear intersection**: Auxiliary planes intersect along a common axis (Fig. 2b). (3) **Partial coplanarity**: Planes b and c are coplanar and parallel to plane a (Fig. 2c). (4) **Coaxial configuration**: Planes b and c are coplanar and parallel to plane a, with coaxial Z_b- and Z_c-axes (Fig. 2d).

3R2T parallel mechanism. This mechanism exhibits three rotational DOFs and two translational DOFs parallel to the X_aY_a-plane, necessitating a constraint force along the Z_g-axis (Fig. 2e). Through screw theory analysis, this constraint condition translates to three constraint forces along coaxial Z_a-, Z_b-, and Z_c-axes, with non-parallel local coordinate axes.

2R3T parallel mechanism. Featuring three translational DOFs and two rotational DOFs parallel to the X_aY_a-plane, this parallel mechanism requires a constraint couple about the Z_g-axis (Fig. 2f). This manifests as constraint couples about each Z_i-axis ($i \in \{a, b, c\}$) within the geometric arrangement shown in Fig. 2c.

3R1T parallel mechanism. Combining three rotational DOFs with one translational DOF along the Z_g-axis requires constraint forces along the X_g-and Y_g-axes (Fig. 2g). This constraint condition can be achieved through either: (1) single constraint forces along the X_i-axis (Fig. 2g) or the Y_i-axis, or (2) dual constraint forces along both X_i- and Y_i-axes for each local frame.

1R3T parallel mechanism. Three translational DOFs with one rotational DOF about the Z_g-axis necessitate constraint couples about X_g- and Y_g-axes (Fig. 2h). Such a constraint condition requires either: (1) single constraint couples about X_i- or Y_i-axes with specific geometric distributions (Figs. 2a, 2b), as shown in Figs. 2h(i) and 2h(ii), respectively, or (2) dual constraint couples about both local axes, as illustrated in Fig. 2h(iii).

2R2T parallel mechanism. Two rotational DOFs parallel to the Y_gZ_g-plane and two translational DOFs parallel to the X_gY_g-plane require a constraint couple about the X_g-axis and a constraint force along the Z_g-axis (Fig. 2i), implemented through constraint forces along each Z_i-axis in the configuration of Fig. 2d.

2R1T parallel mechanism. Two rotational DOFs parallel to the X_gY_g-plane with one translational DOF along Z_g-axis require a constraint couple about the Z_g-axis and forces along the X_g- and Y_g-axes (Fig. 2j), achieved through constraint forces along X_i- or Y_i-axes in the configuration of Fig. 2a.

3T parallel mechanism. Pure translational mobility requires three orthogonal constraint couples (Fig. 2k). This constraint condition is equivalent to either: (1) two constraint couples exist for each local coordinate, one about the Z_g-axis and another about either the X_i- or Y_i-axes, in the configuration of Fig. 2a (constraint conditions are presented in Fig. 2k(i)) or Fig. 2b (constraint conditions are shown in Fig. 2k(ii)), or (2) three constraint couples exist about all local coordinate axes in the configuration of Figs. 2a, 2b, or 2c (equivalent constraint conditions based on local coordinates are shown in Fig. 2k(iii)).

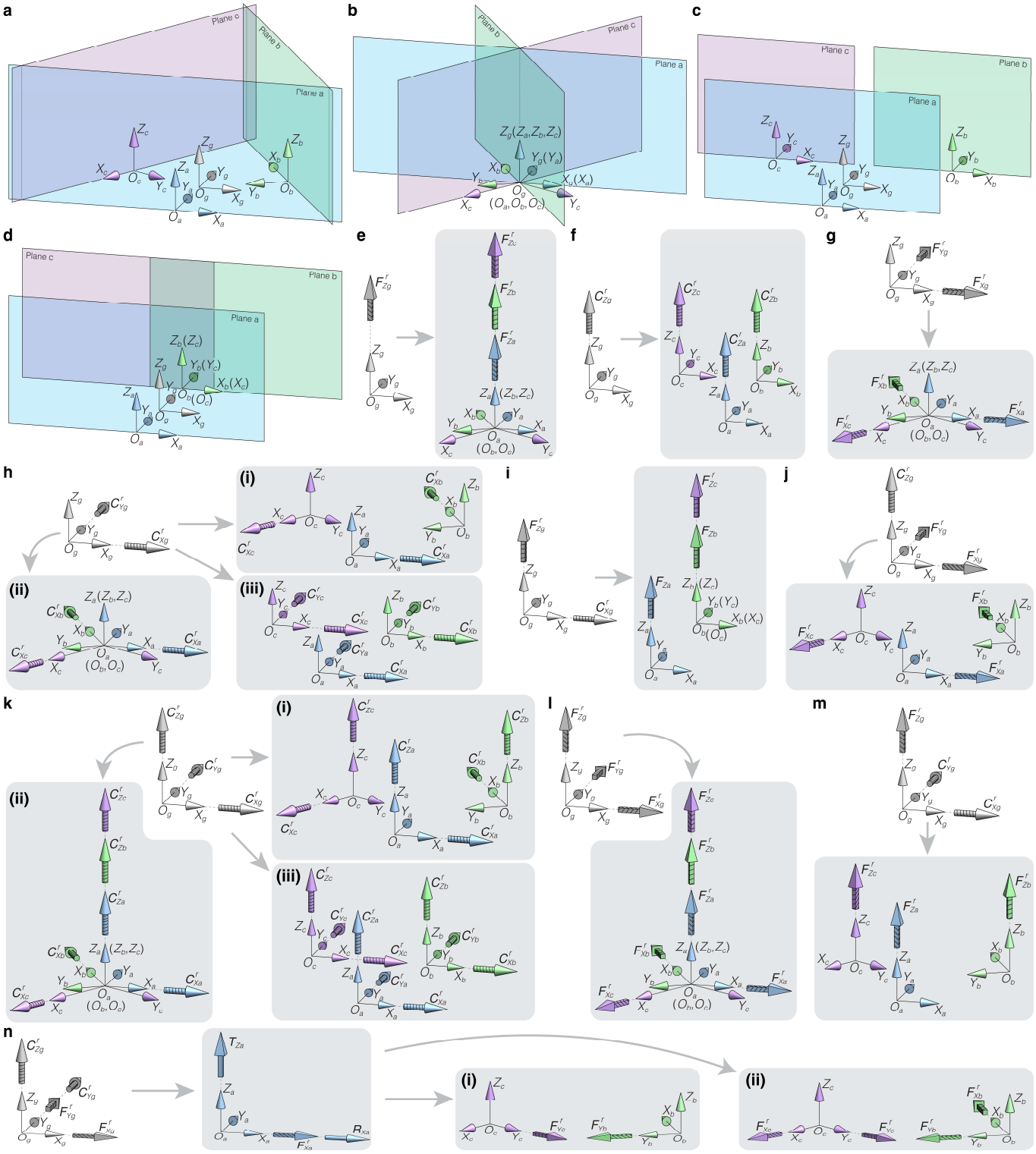

Fig. 2. Relationships between global and local coordinate frames in Task A. **(a)-(d)** Four spatial configurations of coordinate frames. The auxiliary planes a, b, and c are determined by the X_i- and Z_i-axes ($i \in$ {a, b, c}), respectively. In **(a)**, three auxiliary planes form a triangular prism configuration. In **(b)**, three auxiliary planes are collinear, where the Z_i-axes ($i \in$ {a, b, c}) are collinear with the Z_g-axis. In **(c)**, three auxiliary planes are parallel to each other, with non-coincident coordinate origins. In **(d)**, three auxiliary planes are parallel to each other, with the coordinate origin O_b coinciding with O_c. **(e)-(n)** Constraint condition relationships between global and local coordinate frames. **(e)** Constraint force along the Z_g-axis. **(f)** Constraint couple about the Z_g-axis. **(g)** Constraint forces along the X_g- and Y_g-axes. **(h)** Constraint couples about the X_g- and Y$_g$-axes. **(i)** Constraint force along the Z_g-axis and constraint couple about the X_g-axis. **(j)** Constraint forces along the X_g- and Y_g-axes and constraint couple about the Z_g-axis. **(k)** Constraint couples about the X_g-, Y_g-, and Z_g-axes. **(l)** Constraint forces along the X_g-, Y_g-, and Z_g-axes. **(m)** Constraint force along the Z_g-axis and constraint couples about the X_g- and Y_g-axes. **(n)** Constraint forces along the X_g- and Y_g-axes, and constraint couples about the Y_g- and Z_g-axes.

3R parallel mechanism. Pure rotational mobility necessitates three orthogonal constraint forces (Fig. 2l), implemented through either: (1) two constraint forces per local frame, one along the Z_g-axis and another along either the X_i- or Y_i-axes, in the configuration of Fig. 2b, or (2) three constraint forces along all local axes in the configuration of Fig. 2b.

1R2T parallel mechanism. One rotational DOF about the Z_g-axis with two translational DOFs parallel to the X_gY_g-plane requires two constraint couples (about the X_g- and Y_g-axes) and one constraint force (along the Z_g-axis), implemented through constraint forces along each Z_i-axis in the configuration of Fig. 2a.

1R/1T reconfigurable parallel mechanism. This metamorphic mechanism transitions between rotational motion about the X_g-axis and translational motion along the Z_g-axis, exhibiting two DOFs. The constraint system comprises two couples (about the Y_g- and Z_g-axes) and two forces (along the X_g- and Y_g-axes) as shown in Fig. 2n. The metamorphic chain at $\{O_a\text{-}X_aY_aZ_a\}$ provides the required mobility while introducing a constraint force along the X_a-axis. The remaining chains based on the coordinate frames $\{O_b\text{-}X_bY_bZ_b\}$ and $\{O_c\text{-}X_cY_cZ_c\}$ require either: (1) single constraint forces along X_i-axis or Y_i-axis ($i \in \{\mathrm{b}, \mathrm{c}\}$, Fig. 2n(i)), or (2) dual constraint forces along both X_i- and Y_i-axes, as presented in Fig. 2n(ii).

Linear combination of motion-screws (Task B)

In this task, INGRID generates new kinematic joints through systematic combinations of motion-screws. The knowledge base provides the physical interpretation of each motion-screw, enabling INGRID to learn and combine these mathematical representations to synthesize new kinematic joints. To facilitate INGRID's comprehension of the underlying mechanics, we introduce two fundamental concepts: revolute-joint-screws, which represent revolute joints, and prismatic-joint-screws, which characterize prismatic joints. The linear combination process is decomposed into discrete steps, allowing INGRID to systematically understand both the methodology of motion-screw combination and the corresponding kinematic joints.

The motion-screw system's standard base contains six screws ($\boldsymbol{S}_{a1}$, $\boldsymbol{S}_{a2}$, $\boldsymbol{S}_{a3}$, $\boldsymbol{S}_{a4}$, $\boldsymbol{S}_{a5}$, $\boldsymbol{S}_{a6}$) representing three orthogonal rotational and three orthogonal translational DOFs. Following constraint identification in Task A, INGRID eliminates specific motion-screws corresponding to the imposed force or couple constraints, thereby deriving a new motion-screw system (see Supplementary Section 4 for detailed specifications). Subsequently, INGRID combines the retained motion-screws to generate new ones representing new kinematic joints.

Combination using revolute-joint-screws. Three distinct scenarios emerge based on the number of revolute-joint-screws in the standard base. When the system contains one or two revolute-joint-screws, no new kinematic joints are generated. However, with three revolute-joint-screws, INGRID synthesizes multiple kinematic joints: revolute joints with rotation axes passing through the local coordinate origin (denoted as R^g_O), 2R spherical sub-chains (denoted as $(R^iR^j)_N$), or 3R spherical sub-chains (denoted as $(R^iR^jR^k)_N$), as illustrated in Figure 3a. Representative examples are provided in Supplementary Example B1.

Combination using prismatic-joint-screws. Two scenarios enable the generation of new kinematic joints through prismatic-joint-screw combinations. First, when the standard base contains two prismatic-joint-screws, INGRID generates two prismatic joints with translational mobility parallel to a plane defined by two local coordinate axes. Figure 3b illustrates prismatic joints with translational mobility parallel to the X_aY_a-plane, denoted as P^y.

Second, when three prismatic-joint-screws are present, INGRID generates three prismatic-joint-screws whose last three components are non-zero, indicating prismatic joints with arbitrary translational directions, denoted as P^g (Figure 3c). Mathematical derivations and detailed formulations are presented in Supplementary Example B2.

Combination using single revolute-joint-screws with prismatic-joint-screws. INGRID performs linear combinations of individual revolute-joint-screws with prismatic-joint-screws to generate new revolute joints. To prevent screw joint generation, we explicitly exclude combinations of $\boldsymbol{S}_{a1} = (1,0,0,0,0,0)^{\mathrm{T}}$ with $\boldsymbol{S}_{a4} = (0,0,0,1,0,0)^{\mathrm{T}}$, $\boldsymbol{S}_{a2} = (0,1,0,0,0,0)^{\mathrm{T}}$ with $\boldsymbol{S}_{a5} = (0,0,0,0,1,0)^{\mathrm{T}}$, and $\boldsymbol{S}_{a3} = (0,0,1,0,0,0)^{\mathrm{T}}$ with $\boldsymbol{S}_{a6} = (0,0,0,0,0,1)^{\mathrm{T}}$. This constraint yields nine valid combination cases, detailed in Supplementary Section 4.5.

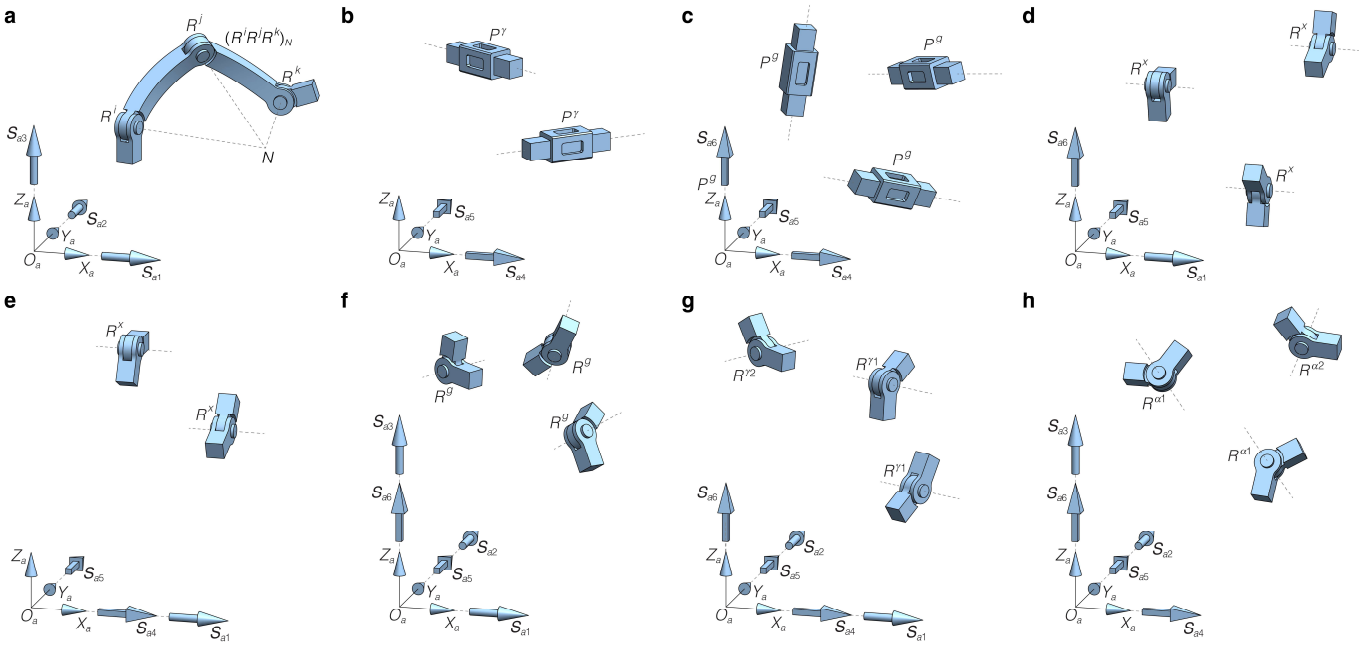

Fig. 3. Construction of new kinematic joints in Task B. **(a)** A 3R spherical joint. **(b)** Two prismatic joints with translational directions parallel to the X_aY_a-plane. **(c)** Three general prismatic joints. **(d)** Three revolute joints with rotational axes parallel to the X_a-axis. **(e)** Two revolute joints with rotational axes parallel to the X_a-axis. **(f)** Three general revolute joints. **(g)** Three revolute joints with rotational axes parallel to the X_aZ_a-plane, two of which are parallel to each other. **(h)** Three revolute joints with rotational axes parallel to the Y_aZ_a-plane, two of which are parallel to each other.

We implement a decision tree to ensure comprehensive generation of potential kinematic joints. When the standard base contains $\boldsymbol{S}_{a1}$ with both $\boldsymbol{S}_{a5}$ and $\boldsymbol{S}_{a6}$, INGRID generates three revolute joints. If only one of $\boldsymbol{S}_{a5}$ or $\boldsymbol{S}_{a6}$ is present, two revolute joints are generated. This logic extends to combinations of $\boldsymbol{S}_{a2}$ with $\boldsymbol{S}_{a4}$ and $\boldsymbol{S}_{a6}$, as well as $\boldsymbol{S}_{a3}$ with $\boldsymbol{S}_{a4}$ and $\boldsymbol{S}_{a5}$.

Figure 3d exemplifies a configuration where the standard base includes $\boldsymbol{S}_{a1}$, $\boldsymbol{S}_{a5}$, and $\boldsymbol{S}_{a6}$, yielding three revolute-joint-screws representing revolute joints with rotational axes parallel to the X_a-axis (denoted as R^x). In Figure 3e, the standard base comprises $\boldsymbol{S}_{a1}$, $\boldsymbol{S}_{a4}$, and $\boldsymbol{S}_{a5}$. Following our exclusion criteria for $\boldsymbol{S}_{a1}$ and $\boldsymbol{S}_{a4}$ combinations, INGRID combines $\boldsymbol{S}_{a1}$ with $\boldsymbol{S}_{a5}$, generating two revolute-joint-screws corresponding to revolute joints with rotational axes parallel to the X_a-axis (R^x). Mathematical formulations are detailed in Supplementary Examples B3 and B4.

Combination using multiple revolute-joint-screws with prismatic-joint-screws. When combining multiple revolute-joint-screws with prismatic-joint-screws, INGRID employs specific criteria to identify valid combinations. Three scenarios are excluded from consideration: (1) The standard base contains three revolute-joint-screws with fewer than two prismatic-joint-screws, which would yield instantaneous kinematic chains. (2) The standard base with two revolute-joint-screws and fewer than three prismatic-joint-screws, where screw theory cannot be used to derive new kinematic joints. (3) The standard base with fewer than two revolute-joint-screws, which preclude new joint generation.

INGRID processes three valid scenarios: (1) *Three revolute-joint-screws with two prismatic-joint-screws*: Figure 3f demonstrates a configuration containing $\boldsymbol{S}_{a1}$, $\boldsymbol{S}_{a2}$, $\boldsymbol{S}_{a3}$, $\boldsymbol{S}_{a5}$, and $\boldsymbol{S}_{a6}$. Linear combination yields three general revolute joints (Supplementary Example B5). (2) *Three revolute-joint-screws with three prismatic-joint-screws*: This case enables the generation of new multiple kinematic joints. (3) *Two revolute-joint-screws with three prismatic-joint-screws*: This combination produces three revolute joints with rotational axes parallel to a plane defined by local coordinate axes. Figure 3g illustrates a combination result excluding $\boldsymbol{S}_{a3}$, generating revolute joints with axes parallel to the X_aZ_a-plane, where two axes are mutually parallel (denoted as $R^{\gamma 1}$, $R^{\gamma 1}$, $R^{\gamma 2}$; see Supplementary Example B6). Figure 3h shows a combination result excluding $\boldsymbol{S}_{a1}$, yielding revolute joints with axes parallel to the Y_aZ_a-plane, again with two parallel axes (denoted as $R^{\alpha 1}$, $R^{\alpha 1}$, $R^{\alpha 2}$; see Example B7).

Through this systematic approach, INGRID generates potential motion-screws representing new kinematic joints. We present seven representative cases demonstrating INGRID's application of screw theory and our prescribed rules (see Movie S1).

Construction of kinematic chains (Task C)

INGRID generates new kinematic chains using potential kinematic joints obtained from Task B. To enable systematic generation of kinematic chains, we introduce two fundamental concepts: P-based sub-chains and R-based sub-chains. Kinematic joints created using prismatic-joint-screws are designated as P-based kinematic joints, even when combined with revolute-joint-screws to form new revolute joints. Conversely, joints generated from multiple revolute-joint-screws, such as $(R^iR^j)_N$ and R^g, are classified as R-based kinematic joints. Thus, P-based sub-chains comprise prismatic joints and revolute joints with axes parallel to the coordinate axes, whereas R-based sub-chains contain revolute joints with specific orientations

In addition, INGRID recognizes that motion screws represent kinematic joints and that sequences of motion screws denote kinematic chains. For example, a five-joint kinematic chain can be represented using five motion-screws; however, not all permutations and combinations yield physically valid chains. Therefore, constructing kinematic chains requires identifying valid permutations of appropriate motion-screws. Each kinematic joint is denoted by a motion-screw and corresponding symbol, with physical meanings detailed in the Supplementary Nomenclature.

To enable INGRID to construct kinematic chains from joints obtained in Task B, we developed a comprehensive rule-based knowledge framework through an iterative training process. Initially, INGRID generates all possible permutations using the available kinematic joints. We subsequently identify and eliminate instantaneous mechanisms from this set. Through systematic refinement, we establish rules that guide INGRID to produce only valid permutations. This iterative process resembles supervised learning, where we derive optimal rules for the knowledge base that enables INGRID to generate correct permutations systematically.

The rule framework consists of four hierarchical categories: joint availability, count constraints, positional requirements, and special case considerations.

Joint identification and availability. First, INGRID identifies available kinematic joints from Task B outputs. For example, if Task B generates P^α, $(R^iR^j)_N$, $(R^iR^jR^k)_N$, R^x, R^y, R^z, and R^g, INGRID categorizes these into R-based joints (i.e. $(R^iR^j)_N$ and $(R^iR^jR^k)_N$), and P-based joints (i.e. P^α and R^x).

Joint count constraints. The total number of kinematic joints equals the number of available motion-screws, as we consider only revolute and prismatic joints that can be represented by single motion-screws. For chains containing one prismatic joint, INGRID evaluates specific configurations identified through our training process:

Case 1: one $(R^iR^j)_N$, two R^x, and one P^α (five joints total).
Case 2: one R^g-R^g, two R^x, and one P^α (five joints total).
Case 3: one $(R^iR^jR^k)_N$, one R^x, and one P^α (five joints total).
Case 4: one R^g-R^g-R^g, one R^x, and one P^α (five joints total).

Positional requirements. Critical rules govern the position of joints within the chain. For example, the fundamental sequence structure in some cases requires: (i) beginning with the base (B), (ii) followed by the P-based kinematic sub-chain (including any R^x joints if present), and (iii) ending with the R-based kinematic sub-chain. Additional constraints include the requirement that three $R^{\gamma 1}$ joints must be connected consecutively, with no permutations allowing $R^{\gamma 2}$ to appear between two $R^{\gamma 1}$ joints. To reduce hallucination rates in large language models, we provide valid base arrangements (for example, B-$R^{\gamma 1}$-$R^{\gamma 1}$-$R^{\gamma 2}$ and B-$R^{\gamma 2}$-$R^{\gamma 1}$-$R^{\gamma 1}$) that allow INGRID to insert specific joints systematically.

Special case rules. Through comprehensive analysis, we identified additional permutations beyond the basic rules. These special rules considerably broaden the solution space. For $(R^iR^j)_N$ joints, the sub-chain $P^{\alpha 2}$-$(R^iR^j)_N$ generates an additional permutation: $P^{\alpha 2}{}_N$-$P^{\alpha 2}$-$R^j{}_N$. Similarly, for $(R^iR^jR^k)_N$ joints, the sub-chain $P^{\alpha 2}$-$(R^iR^jR^k)_N$ produces the permutation $P^{\alpha 2}{}_N$-$P^{\alpha 2}$-$(R^jR^k)_N$. These rules enable INGRID to discover new permutations not previously documented in the literature.

Implementation and validation. INGRID carries out this task based on the diverse outputs from Task B, making slight adjustments to the count and position rules to accommodate different configurations. Detailed rules and prompts are provided in the Supplementary Section 5. Movie S2 demonstrates 13 representative cases, illustrating how INGRID systematically generates valid permutations from given inputs. This visualization demonstrates the procedure by which INGRID systematically generates a complete set of valid permutations based on the specified input.

Design of Robotic Mechanisms (Task D)

We demonstrate the application of our framework through three case studies of parallel robotic mechanism design. In each case, INGRID generates new kinematic configurations that satisfy user-specified mobility requirements while maintaining structural validity.

2R1T parallel mechanism. The first case study targets a mechanism with two rotational and one translational DOFs. Following the framework's knowledge-based prompts, three local coordinate frames were established with specific orientations (Fig. 4a). In Task A, INGRID identified the required constraint conditions: one constraint couple about the Z_g-axis and two constraint forces along the X_g- and Y_g-axes. These global constraints map to a single constraint force along each local X_l-axis, as shown in Fig. 4b.

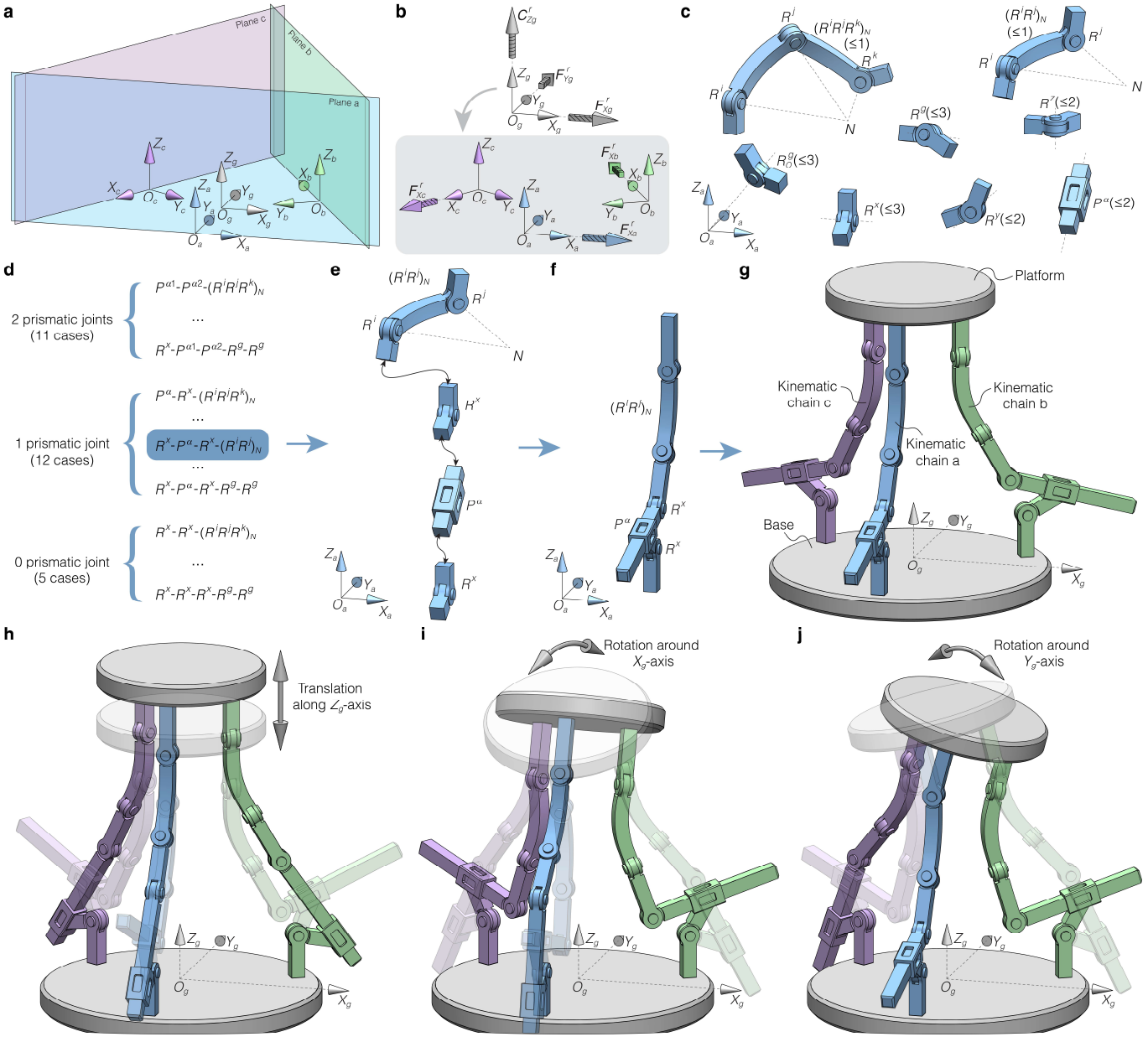

Fig. 4. Design process of the 2R1T parallel mechanism. **(a)** INGRID identifies the distribution of global and three local coordinate frames. **(b)** Constraint conditions in local coordinates derived from the global coordinate frame. **(c)** New kinematic joints in the local coordinate frame $\{O_a\text{-}X_aY_aZ_a\}$. **(d)** INGRID generates 28 permutations using candidate kinematic joints. **(e)-(f)** The $R^x\text{-}P^\alpha\text{-}R^x\text{-}(R^iR^j)_N$ chain is selected as an example to construct a new kinematic chain. **(g)** A parallel mechanism designed using the new kinematic chain. **(h)-(j)** Three motion demonstrations of the parallel mechanism: translational motion along the Z_g-axis, and rotational motions about the X_g- and Y_g-axes, respectively.

In Task B, INGRID generated feasible kinematic joint configurations for the local frame $\{O_a\text{-}X_aY_aZ_a\}$. The system identified eight joint types (Fig. 4c): spherical joints $(R^iR^jR^k)_N$ and $(R^iR^j)_N$, general revolute joints R^g, axis-specific revolute joints (R^x, R^y, R^z), revolute joints through origin $R^g{}_O$, and prismatic joints P^α.

From the generated permutations (Fig. 4d), we selected the configuration $R^x\text{-}P^\alpha\text{-}R^x\text{-}(R^iR^j)_N$ to construct a kinematic chain (Figs. 4e-f) and assembled the complete parallel mechanism (Fig. 4g). Validation confirmed the mechanism's designed mobility: translation along the Z_g-axis (Fig. 4h), and rotation about the X_g-axis (Fig. 4i) and Y_g-axis (Fig. 4j), respectively.

1R3T parallel mechanism. The second case study shows a mechanism with one rotational and three translational DOFs. The constraint analysis yields two constraint couples about the X_g- and Y_g-axes, equivalent to one constraint couple along each local X_i-axis (Figs. 5a-b).

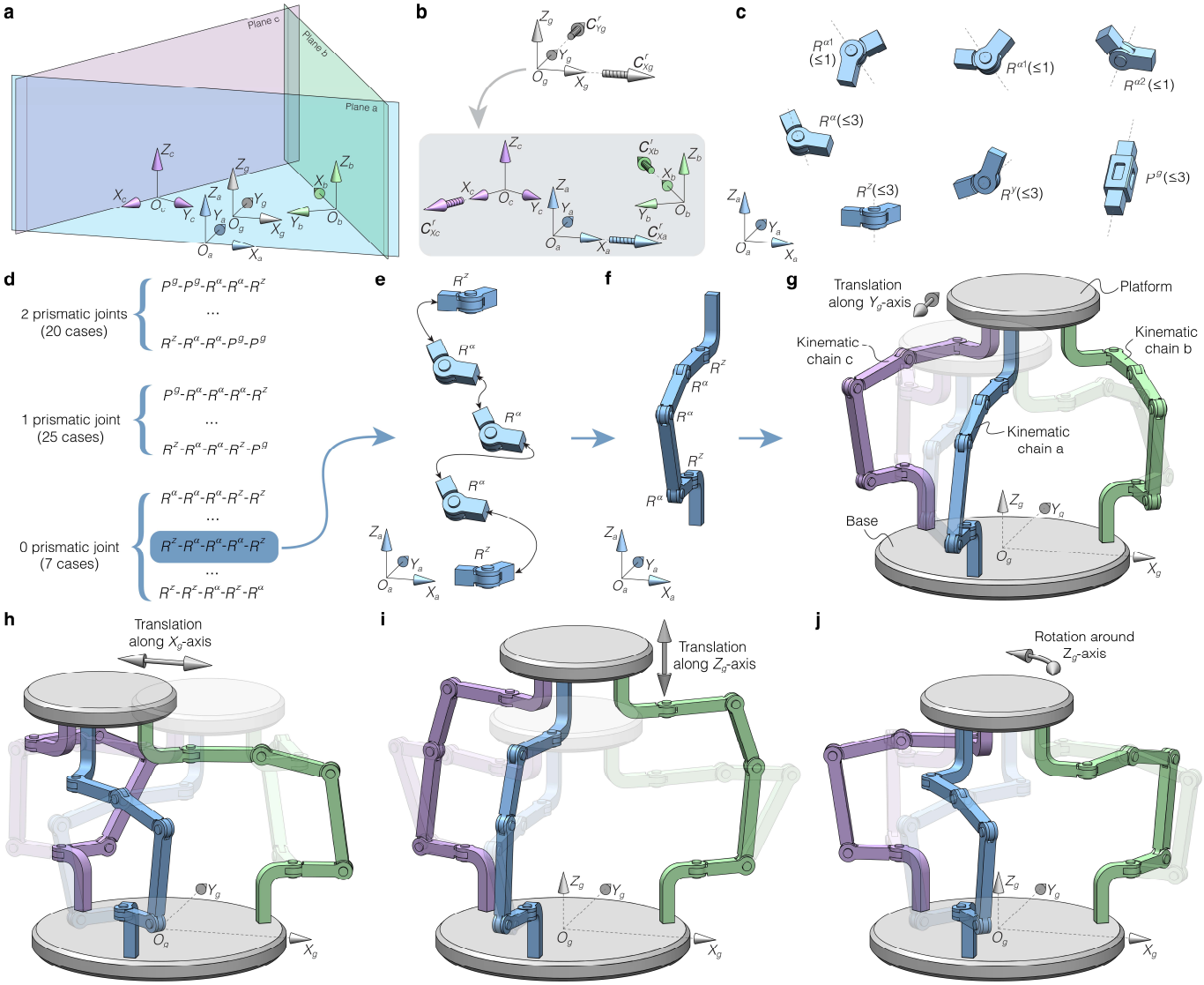

Fig. 5. Design process of the 1R3T parallel mechanism. **(a)** INGRID identifies the distribution of global and three local coordinate frames. **(b)** Constraint conditions in local coordinates derived from the global coordinate frame. **(c)** New kinematic joints in the local coordinate frame $\{O_a\text{-}X_aY_aZ_a\}$. **(d)** INGRID generates 52 permutations using candidate kinematic joints. **(e)-(f)** The $R^z\text{-}P^\alpha\text{-}P^\alpha\text{-}P^\alpha\text{-}R^z$ chain is selected as an example to construct a new kinematic chain. **(g)** A parallel mechanism designed using the new kinematic chain. **(h)-(k)** Four motion demonstrations of the parallel mechanism: translational motions along the X_g-, Y_g-, and Z_g-axes, and rotational motion about the Z_g-axis, respectively.

In Task B, INGRID generated new kinematic joints based on the local coordinate frames, including revolute joints with axes parallel to the Y_aZ_a-plane (R^{α}), specially constrained revolute joints ($R^{\alpha 1}$ & R^{α} & $R^{\alpha 2}$) where two axes are parallel, axis-aligned revolute joints (R^{y}, R^{z}), and general prismatic joints (P^{g}) (Fig. 5c).

We selected the R^{z}-P^{α}-P^{α}-P^{α}-R^{z} configuration (Figs. 5d-f) to construct the parallel mechanism (Fig. 5g). Validation demonstrated full spatial translation capability along all three axes (Figs. 5g-i) and rotation about the Z_g-axis (Fig. 5j). The detailed process can be seen in Movie S3.

1R/1T reconfigurable parallel mechanism. The third case study presents a reconfigurable mechanism switching between rotational and translational mobility. The auxiliary planes form a triangular prism configuration (Fig. 6a). Following established design principles [46, 47], the primary kinematic chain (Fig. 6b) provides translational mobility along the Z_a-axis and rotational mobility about the X_a-axis, while introducing a constraint force along the X_a-axis.

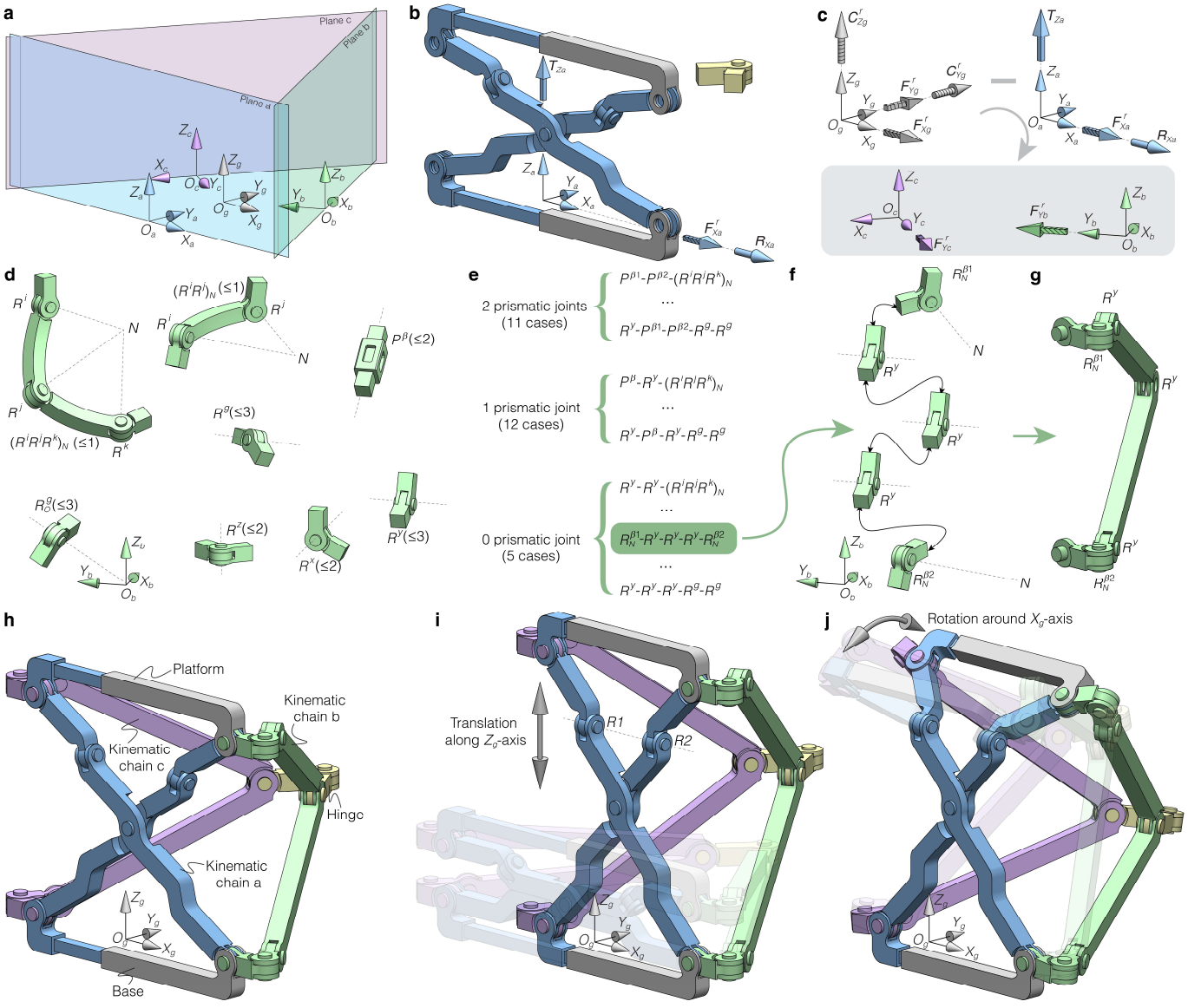

Fig. 6. Design process of the 1R1T reconfigurable parallel mechanism. **(a)** INGRID identifies the distribution of global and three local coordinate frames. **(b)** The reconfigurable sub-mechanism and desired mobility in the local coordinate frame $\{O_a\text{-}X_aY_aZ_a\}$. **(c)** Constraint conditions in the local coordinate frames $\{O_b\text{-}X_bY_bZ_b\}$ and $\{O_c\text{-}X_cY_cZ_c\}$ are derived from the global coordinate frame and the local coordinate frame $\{O_a\text{-}X_aY_aZ_a\}$. **(d)** New kinematic joints in the local coordinate frame $\{O_b\text{-}X_bY_bZ_b\}$. **(e)** INGRID generates 28 new kinematic chains using candidate kinematic joints. **(f)-(g)** The $R^{\beta 1}{}_N$-R^{y}-R^{y}-R^{y}-$R^{\beta 2}{}_N$ chain is selected as an example to construct a new kinematic chain. **(h)** A reconfigurable parallel mechanism designed using the new kinematic chain. **(i)-(j)** Two motion demonstrations of the reconfigurable parallel mechanism: translational motion along the Y_g-axis and rotational motion about the X_g-axis, respectively.

To achieve the required global constraints, two constraint forces along the X_g- and Y_g-axes and two constraint couples about the Y_g- and Z_g-axes are needed (Fig. 6c). The framework shows that the constraint forces along the Y_i-axis (i ∈ {b, c}) satisfy these requirements when combined with the primary kinematic chain constraints.

Subsequently, INGRID carried out Task B and generated joint configurations for the local coordinate frame $\{O_b\text{-}X_bY_bZ_b\}$, including spherical joints, axis-aligned revolute joints, and planar prismatic joints P^{β} (Fig. 6d). From the valid permutations (Fig. 6e), we selected $R^{\beta 1}{}_N\text{-}R^y\text{-}R^y\text{-}R^y\text{-}R^{\beta 2}{}_N$ for the secondary chains (Figs. 6f-g).

The assembled mechanism consists of one primary chain and two plane-symmetric secondary chains connected via a central hinge (Fig. 6h). The mechanism exhibits single-degree-of-freedom reconfigurable behavior: when $R1$ and $R2$ axes are non-collinear, the platform translates along the Z_g-axis (Fig. 6i); when collinear, rotation about the aligned axis becomes possible while translation is constrained. The detailed synthesis process and simulation are shown in Movie S3.

Discussion

INGRID represents a paradigm shift in mechanism design by integrating large language models with established kinematic synthesis principles. The system encodes screw theory fundamentals, constraint analysis methods, and motion-screws combination rules into a structured knowledge base accessible to language models, enabling systematic generation of kinematic chains from natural language specifications. This approach parallels successful applications in other domains: Generative Pre-trained Transformer (GPT) models generate sentences based on learned grammatical rules, and AlphaFold [48-50] predicts protein structures from amino acid sequences. Similarly, INGRID synthesizes robotic mechanisms from kinematic joints by applying learned design principles.

Our experimental validation demonstrates that INGRID successfully generates functional parallel mechanisms, including both traditional fixed-mobility designs and reconfigurable systems. The system exhibits doctoral-level expertise in mechanism design, systematically exploring the design space to discover new mechanism configurations. By maintaining successful designs and synthesis strategies in an expanding knowledge base, INGRID facilitates knowledge transfer and accumulation across design iterations.

The current implementation has several limitations that define future research directions. First, INGRID currently considers only lower pairs, including prismatic and revolute joints, and excludes universal, cylindrical, and other joint types. Second, while the system generates comprehensive lists of kinematic joint permutations for parallel mechanisms, it cannot yet produce URDF files directly. These limitations can be addressed through the systematic expansion of the knowledge base. Incorporating additional joint types requires extending the prompt library and synthesis rules. Automatic URDF generation can be achieved by integrating established methods, such as Denavit-Hartenberg parameters, with additional training examples.

Despite these constraints, INGRID demonstrates the feasibility of LLM-driven mechanism design. The system's ability to perform type synthesis and enumerate new kinematic chains validates its potential for fully automated robotic design. By bridging natural language and mechanism synthesis, this work advances both mechanism design and the broader vision of machine intelligence—developing AI systems that are capable of designing, rather than merely controlling, their physical embodiments. Future research will focus on experimental validation in practical domains, including de novo design applications and integration with physics-informed constraints to ensure the realizability of generated mechanisms.

Methods

System Architecture and Implementation. We implemented the INGRID system using LLMs with structured prompt engineering. The system architecture comprises five modular text files: one containing fundamental concepts, symbol definitions, and physical interpretations, and four task-specific modules (Tasks A–D). These files were uploaded to Claude Sonnet 4 and Claude Opus 4.1, along with the complete workflow protocol. The system autonomously generates permutations representing novel kinematic chains, with all processes documented in Supplementary Movies.

Screw Theory Integration. We provided comprehensive theoretical foundations to enable INGRID's understanding of screw theory and derivation of constraint screws using reciprocal screw principles (Supplementary Section 2). The training materials included fundamental concepts of screws, constraint screws, and reciprocal screw theory. Additionally, we incorporated

detailed rules governing linear combinations of motion-screws to facilitate comprehension of the procedures outlined in Supplementary Sections 4.1 and 4.2 (Task B, Step B1).

Linear combination optimization for single revolute joints. During system training, we identified systematic errors in INGRID's handling of linear combinations involving single revolute-joint-screws combined with prismatic-joint-screws. The system exhibited two primary failure modes: incomplete combination generation (e.g., combining $\boldsymbol{S}_{a1}$ with $\boldsymbol{S}_{a5}$ while omitting $\boldsymbol{S}_{a1}$ with $\boldsymbol{S}_{a6}$ from the standard motion-screw base $\{\boldsymbol{S}_{a1}, \boldsymbol{S}_{a5}, \boldsymbol{S}_{a6}\}$) and redundant processing (generating four revolute-joint-screws instead of the correct three through sequential pairwise combinations). To address these limitations, we developed a decision tree algorithm (Supplementary Section 4.5) that ensures systematic generation of exactly three new revolute-joint-screws through simultaneous linear combination of $\boldsymbol{S}_{a1}$ with both $\boldsymbol{S}_{a5}$ and $\boldsymbol{S}_{a6}$.

Permutation enumeration using kinematic notation. We implemented a three-stage validation process for kinematic chain synthesis. First, we analyzed Task B outputs and identified 13 valid cases suitable for Task C input, excluding configurations that produce instantaneous mechanisms or lack sufficient kinematic joints for mechanism construction. Second, we characterized the available kinematic joints from Task B and identified those unsuitable for valid permutation construction. We then trained INGRID to select appropriate kinematic joints in Step C1 (Supplementary Section 5). Third, we train INGRID to generate comprehensive permutations using available joints, followed by elimination of instantaneous configurations and those that lose essential properties under finite motion. The complete derivation process is presented in Movie S2.

Robotic mechanism construction and validation. While INGRID successfully performs type synthesis autonomously by generating valid kinematic chain permutations, direct mechanism construction requires additional spatial information beyond joint sequence and type data. We addressed this limitation by incorporating positional parameters into kinematic chains, enabling assembly with platforms and bases to create complete parallel robotic mechanisms in SolidWorks. Models were converted to URDF format using dedicated plugins and imported into Isaac Sim for verification of mobility. The complete construction and validation workflow is demonstrated in Movies S3-S5.

References

[1] A. Billard, A. Albu-Schaeffer, M. Beetz, W. Burgard, P. Corke, M. Ciocarlie, R. Dahiya, D. Kragic, K. Goldberg, Y. Nagai, and D. Scaramuzza, A roadmap for AI in robotics, Nat. Mach. Intell. 7 (6) (2025) 818-824.
[2] T. F. Nygaard, C. P. Martin, J. Torresen, K. Glette, and D. Howard, Real-world embodied AI through a morphologically adaptive quadruped robot, Nat. Mach. Intell. 3 (5) (2021) 15.
[3] Y. B. Jin, X. W. Liu, Y. C. Shao, H. T. Wang, and W. Yang, High-speed quadrupedal locomotion by imitation-relaxation reinforcement learning, Nat. Mach. Intell. 4 (12) (2022) 1198-1208.
[4] M. Thor, and P. Manoonpong, Versatile modular neural locomotion control with fast learning, Nat. Mach. Intell. 4 (2) (2022) 169-179.
[5] W. M. Yu, C. Y. Yang, C. McGreavy, E. Triantafyllidis, G. Bellegarda, M. Shafiee, A. J. Ijspeert, and Z. B. Li, Identifying important sensory feedback for learning locomotion skills, Nat. Mach. Intell. 5 (8) (2023) 919-+.
[6] L. Han, Q. X. Zhu, J. P. Sheng, C. Zhang, T. G. Li, Y. Z. Zhang, H. Zhang, Y. Z. Liu, C. Zhou, R. Zhao, J. Li, Y. F. Zhang, R. Wang, W. C. Chi, X. Li, Y. H. Zhu, L. Z. Xiang, X. Teng, and Z. Y. Zhang, Lifelike agility and play in quadrupedal robots using reinforcement learning and generative pre-trained models, Nat. Mach. Intell. 6 (7) (2024) 14.
[7] F. Stella, M. M. Achkar, C. Della Santina, and J. Hughes, Synergy-based robotic quadruped leveraging passivity for natural intelligence and behavioural diversity, Nat. Mach. Intell. 7 (3) (2025) 20.
[8] L. Johannsmeier, S. Schneider, Y. N. Li, E. Burdet, and S. Haddadin, A process-centric manipulation taxonomy for the organization, classification and synthesis of tactile robot skills, Nat. Mach. Intell. 7 (6) (2025) 916-927.
[9] H. W. Wan, Y. H. Zhang, J. J. Wang, D. H. Wu, M. K. Li, X. L. Chen, Y. X. Deng, Y. X. Huang, Z. L. Sun, L. Zhang, and X. Q. Ji, Toward Universal Embodied Planning in Scalable Heterogeneous Field Robots Collaboration and Control, Journal of Field Robotics 42 (5) (2025) 2318-2336.
[10] J. Y. Chen, E. H. T. Teo, and K. Yao, Electromechanical Actuators for Haptic Feedback with Fingertip Contact, Actuators 12 (3) (2023) 16 104.
[11] R. J. Kirschner, K. Karacan, A. Melone, and S. Haddadin, Categorizing robots by performance fitness into the tree of robots, Nat. Mach. Intell. 7 (3) (2025) 21.
[12] Y. Li, G. Carboni, F. Gonzalez, D. Campolo, and E. Burdet, Differential game theory for versatile physical human-robot interaction, Nat. Mach. Intell. 1 (1) (2019) 36-43.
[13] S. Mintchev, M. Salerno, A. Cherpillod, S. Scaduto, and J. Paik, A portable three-degrees-of-freedom force feedback origami robot for human-robot interactions, Nat. Mach. Intell. 1 (12) (2019) 584-593.

[14] L. Massari, G. Fransvea, J. D'Abbraccio, M. Filosa, G. Terruso, A. Aliperta, G. D'Alesio, M. Zaltieri, E. Schena, E. Palermo, E. Sinibaldi, and C. M. Oddo, Functional mimicry of Ruffini receptors with fibre Bragg gratings and deep neural networks enables a bio-inspired large-area tactile-sensitive skin, Nat. Mach. Intell. 4 (5) (2022) 425-+.
[15] Y. H. Hu, J. Lin, and H. Lipson, Teaching robots to build simulations of themselves, Nat. Mach. Intell. 7 (3) (2025) 17.
[16] H. Ju, R. S. Juan, R. Gomez, K. Nakamura, and G. L. Li, Transferring policy of deep reinforcement learning from simulation to reality for robotics, Nat. Mach. Intell. 4 (12) (2022) 1077-1087.
[17] H. B. Luo, J. X. Wu, J. J. Liu, and M. F. Antwi-Afari, Large language model-based code generation for the control of construction assembly robots: A hierarchical generation approach, Dev. Built Environ. 19 (2024) 18 100488.
[18] S. Schmidgall, J. W. Kim, A. Kuntz, A. E. Ghazi, and A. Krieger, General-purpose foundation models for increased autonomy in robot-assisted surgery, Nat. Mach. Intell. 6 (11) (2024) 1275-1283.
[19] R. Mon-Williams, G. Li, R. Long, W. Q. Du, and C. G. Lucas, Embodied large language models enable robots to complete complex tasks in unpredictable environments, Nat. Mach. Intell. 7 (4) (2025) 592-601.
[20] H. T. Wu, W. Wei, S. H. Li, and M. Y. Chen, Developing a Consumer Electronics Robotics With a Large Language Model Based on a Trustworthy AI Framework, IEEE Trans. Consum. Electron. 71 (1) (2025) 2027-2038.
[21] Z. Huang, and Q. C. Li, General methodology for type synthesis of symmetrical lower-mobility parallel manipulators and several novel manipulators, International Journal of Robotics Research 21 (2) (2002) 131-145.
[22] Z. Huang, and Q. C. Li, Type synthesis of symmetrical lower-mobility parallel mechanisms using the constraint-synthesis method, International Journal of Robotics Research 22 (1) (2003) 59-79.
[23] T. S. Zhao, J. S. Dai, and Z. Huang, Geometric synthesis of spatial parallel manipulators with fewer than six degrees of freedom, Proceedings of the Institution of Mechanical Engineers Part C-Journal of Mechanical Engineering Science 216 (12) (2002) 1175-1185.
[24] D. X. Zeng, and Z. Huang, Type synthesis of the rotational decoupled parallel mechanism based on screw theory, Science China-Technological Sciences 54 (4) (2011) 998-1004.
[25] X. W. Kong, X. Y. He, and T. Kostalas, Type Synthesis of a Novel Class of One-DOF Multi-Mode Parallel Mechanisms, J. Mech. Robot. 17 (4) (2025) 6 044504.
[26] B. Hu, and P. Bai, Type synthesis of 2T1H parallel mechanisms without helical joints based on analytic formulation of screw type terminal constraints, Mech. Mach. Theory 208 (2025) 22 105954.
[27] Z. M. Chen, X. W. Kong, C. Zhao, and Z. Huang, Type synthesis of 3-RSR equivalent 2R1T parallel mechanisms based on screw theory, Mech. Mach. Theory 211 (2025) 18 106032.
[28] H. P. Chu, Y. L. Zhou, and J. T. Yao, Type synthesis of metamorphic parallel robots based on the serial-chain database, Mech. Mach. Theory 181 (2023) 23 105207.
[29] Y. Liu, Y. Z. Li, Y. A. Yao, and X. W. Kong, Type synthesis of multi-mode mobile parallel mechanisms based on refined virtual chain approach, Mech. Mach. Theory 152 (2020) 17 103908.
[30] C. X. Tian, Y. F. Fang, and S. Guo, Structural synthesis of a class of 2R2T hybrid mechanisms, Chinese Journal of Mechanical Engineering 29 (4) (2016) 703-709.
[31] Q. C. Li, and J. M. Hervé, Parallel Mechanisms With Bifurcation of Schoenflies Motion, IEEE Trans. Robot. 25 (1) (2009) 158-164.
[32] Q. C. Li, Z. Huang, and J. M. Hervé, Type synthesis of 3R2T 5-DOF parallel mechanisms using the lie group of displacements, Ieee Transactions on Robotics and Automation 20 (2) (2004) 173-180.
[33] Q. C. Li, and J. M. Herve, Type Synthesis of 3-DOF RPR-Equivalent Parallel Mechanisms, IEEE Trans. Robot. 30 (6) (2014) 1333-1343.
[34] Y. H. Xing, C. X. Tian, Z. H. Xia, J. Gu, and D. Zhang, The novel synthesis of generalized parallel manipulators with 8R Kirigami-inspired configurable platform, Mech. Mach. Theory 209 (2025) 24 106003.
[35] J. Wei, and J. S. Dai, Lie Group Based Type Synthesis Using Transformation Configuration Space for Reconfigurable Parallel Mechanisms With Bifurcation Between Spherical Motion and Planar Motion, J. Mech. Des. 142 (6) (2020) 13 063302.
[36] M. V. Yazici, M. Kocak, T. Uslu, and E. Gezgin, Structural Synthesis of Platform Type Manipulators via Connection-Based Adjacency Matrix: Topology Generation, J. Mech. Des. 147 (1) (2025) 14 013302.
[37] Z. H. Xia, C. X. Tian, L. Q. Li, and D. Zhang, The novel synthesis of mechanisms for continuous origami based on the topological graph theory, Mech. Mach. Theory 204 (2024) 22 105857.
[38] Z. H. Xia, C. X. Tian, L. Q. Li, and D. Zhang, The novel synthesis of origami-inspired mechanisms based on graph theory, Mech. Mach. Theory 192 (2024) 19 105547.
[39] R. F. Lin, W. Z. Guo, and S. S. Cheng, Type synthesis of novel 1R, 2R, 1R1T, and 2R1T hybrid RCM mechanisms based on topological arrangement and modular design method, Mech. Mach. Theory 200 (2024) 28 105692.
[40] N. C. Archer, and J. B. Hopkins, Analysis and synthesis of interconnected hybrid mechanisms using Freedom and Constraint Topologies (FACT), Mech. Mach. Theory 200 (2024) 26 105722.
[41] Y. Z. Zhao, Y. C. Cao, X. W. Kong, and T. S. Zhao, Type Synthesis of Parallel Mechanisms With a Constant Jacobian Matrix, J. Mech. Robot. 10 (6) (2018) 10 061011.
[42] Z. H. Xia, C. X. Tian, Y. H. Xing, J. Gu, L. Q. Li, and D. Zhang, The novel synthesis method of decoupled generalized parallel mechanisms based on motion transmission, Mech. Mach. Theory 210 (2025) 23 106019.

[43] C. X. Tian, Z. H. Xia, L. Q. Li, and D. Zhang, The novel synthesis of reconfigurable generalized parallel manipulators with kinematic redundancy, Mech. Mach. Theory 201 (2024) 16 105748.
[44] Y. Liu, W. J. Lu, D. B. Fan, W. J. Tan, B. Hu, and D. X. Zeng, Type Synthesis of Self-Alignment Parallel Ankle Rehabilitation Robot with Suitable Passive Degrees of Freedom, Chinese Journal of Mechanical Engineering 37 (1) (2024) 16 21.
[45] S. B. Liu, J. P. Mei, P. F. Wang, F. Guo, J. X. Li, S. Wang, and R. Z. Wang, Type Synthesis of a 3DOF Wrist Applying the Coupled-Input Cable-Driven Parallel Robot, J. Mech. Robot. 16 (12) (2024) 11 124502.
[46] G. Jia, B. Li, H. Huang, and D. Zhang, Type synthesis of metamorphic mechanisms with scissor-like linkage based on different kinds of connecting pairs, Mech. Mach. Theory 151 (2020) 103848.
[47] G. Jia, H. Huang, S. Wang, and B. Li, Type synthesis of plane-symmetric deployable grasping parallel mechanisms using constraint force parallelogram law, Mech. Mach. Theory 161 (2021) 104330.
[48] J. Jumper, R. Evans, A. Pritzel, T. Green, M. Figurnov, O. Ronneberger, K. Tunyasuvunakool, R. Bates, A. Zídek, A. Potapenko, A. Bridgland, C. Meyer, S. A. A. Kohl, A. J. Ballard, A. Cowie, B. Romera-Paredes, S. Nikolov, R. Jain, J. Adler, T. Back, S. Petersen, D. Reiman, E. Clancy, M. Zielinski, M. Steinegger, M. Pacholska, T. Berghammer, S. Bodenstein, D. Silver, O. Vinyals, A. W. Senior, K. Kavukcuoglu, P. Kohli, and D. Hassabis, Highly accurate protein structure prediction with AlphaFold, Nature 596 (7873) (2021) 583-+.
[49] M. Varadi, S. Anyango, M. Deshpande, S. Nair, C. Natassia, G. Yordanova, D. Yuan, O. Stroe, G. Wood, A. Laydon, A. Zídek, T. Green, K. Tunyasuvunakool, S. Petersen, J. Jumper, E. Clancy, R. Green, A. Vora, M. Lutfi, M. Figurnov, A. Cowie, N. Hobbs, P. Kohli, G. Kleywegt, E. Birney, D. Hassabis, and S. Velankar, AlphaFold Protein Structure Database: massively expanding the structural coverage of protein-sequence space with high-accuracy models, Nucleic Acids Res. 50 (D1) (2022) D439-D444.
[50] J. Abramson, J. Adler, J. Dunger, R. Evans, T. Green, A. Pritzel, O. Ronneberger, L. Willmore, A. J. Ballard, J. Bambrick, S. W. Bodenstein, D. A. Evans, C. C. Hung, M. O'Neill, D. Reiman, K. Tunyasuvunakool, Z. Wu, A. Zemgulyte, E. Arvaniti, C. Beattie, O. Bertolli, A. Bridgland, A. Cherepanov, M. Congreve, A. I. Cowen-Rivers, A. Cowie, M. Figurnov, F. B. Fuchs, H. Gladman, R. Jain, Y. A. Khan, C. M. R. Low, K. Perlin, A. Potapenko, P. Savy, S. Singh, A. Stecula, A. Thillaisundaram, C. Tong, S. Yakneen, E. D. Zhong, M. Zielinski, A. Zídek, V. Bapst, P. Kohli, M. Jaderberg, D. Hassabis, and J. M. Jumper, Accurate structure prediction of biomolecular interactions with AlphaFold 3, Nature 630 (8016) (2024) 24.